LETTER

doi:10.1038/nature12186

Hofstadter's butterfly and the fractal quantum Hall effect in moiré superlattices

C. R. Dean[1], L. Wang[2], P. Maher[3], C. Forsythe[3], F. Ghahari[3], Y. Gao[2], J. Katoch[4], M. Ishigami[4], P. Moon[5], M. Koshino[5], T. Taniguchi[6], K. Watanabe[6], K. L. Shepard[7], J. Hone[2] & P. Kim[3]

Electrons moving through a spatially periodic lattice potential develop a quantized energy spectrum consisting of discrete Bloch bands. In two dimensions, electrons moving through a magnetic field also develop a quantized energy spectrum, consisting of highly degenerate Landau energy levels. When subject to both a magnetic field and a periodic electrostatic potential, two-dimensional systems of electrons exhibit a self-similar recursive energy spectrum[1]. Known as Hofstadter's butterfly, this complex spectrum results from an interplay between the characteristic lengths associated with the two quantizing fields[1–10], and is one of the first quantum fractals discovered in physics. In the decades since its prediction, experimental attempts to study this effect have been limited by difficulties in reconciling the two length scales. Typical atomic lattices (with periodicities of less than one nanometre) require unfeasibly large magnetic fields to reach the commensurability condition, and in artificially engineered structures (with periodicities greater than about 100 nanometres) the corresponding fields are too small to overcome disorder completely[11–17]. Here we demonstrate that moiré superlattices arising in bilayer graphene coupled to hexagonal boron nitride provide a periodic modulation with ideal length scales of the order of ten nanometres, enabling unprecedented experimental access to the fractal spectrum. We confirm that quantum Hall features associated with the fractal gaps are described by two integer topological quantum numbers, and report evidence of their recursive structure. Observation of a Hofstadter spectrum in bilayer graphene means that it is possible to investigate emergent behaviour within a fractal energy landscape in a system with tunable internal degrees of freedom.

The total number of electron states per area of a completely filled Bloch band is $n_0 = 1/A$, where A is the area of the unit cell of the periodic potential. In a magnetic field, B, the number of states per area of each filled Landau level is given by B/ϕ_0, where $\phi_0 = h/e$ is the magnetic flux quantum (h, Planck's constant; e, magnitude of the electron charge). The quantum description of electrons subjected simultaneously to both a periodic electric field and a magnetic field can be simply parameterized by the dimensionless ratio ϕ/ϕ_0, where $\phi = BA$ is the magnetic flux per unit cell. The general solution, however, exhibits a rich complexity due to the incommensurate periodicities of the Bloch and Landau states[18]. For commensurate fields, corresponding to rational values of $\phi/\phi_0 = p/q$, where p and q are co-prime integers, the single-particle Bloch band splits into q subbands[1] (beginning with the Landau level description, it can be shown that, equivalently, the energy diagram is parameterized by $\phi_o/\phi = q/p$ such that at these same rational values each Landau level splits into p subbands[2]). This results in a quasi-continuous distribution of incommensurate quantum states with a self-similar recursive structure, yielding a butterfly-like fractal energy diagram called the Hofstadter buttefly[1] (Supplementary Information).

Important insight into this system came from consideration of the density of charge carriers, n, required to fill each fractal subband[2]. Replotting the Hofstadter energy spectrum as integrated density versus field shows that all spectral gaps are constrained to linear trajectories in the density–field diagram (Wannier diagram). This can be described by a simple Diophantine relation

$$(n/n_o) = t(\phi/\phi_o) + s \quad (1)$$

where n/n_o and ϕ/ϕ_o are the normalized carrier density and magnetic flux, respectively, and s and t are both integer valued. Here n/n_o represents the Bloch band filling fraction, which is distinct from the usual Landau level filling fraction, $\nu = n\phi_0/B$ (the two are related by the normalized flux, that is, $n/n_o = \nu\phi/\phi_o$). The physical significance of the quantum numbers s and t became fully apparent with the discovery of the integer quantum Hall effect[19] (QHE), after which it was shown that the Hall conductivity associated with each minigap in the fractal spectrum is quantized according to the relation $\sigma_{xy} = te^2/h$ (refs 3, 4). The second quantum number, s, physically corresponds to the Bloch band filling index in the fractal spectrum[5]. This formalism suggests several unique and unambiguous experimental signatures associated with the Hofstadter energy spectrum that are distinct from the conventional QHE. First, the Hall conductance can vary non-monotonically and can even fluctuate in sign. Second, the Hall conductance plateaux, together with vanishing longitudinal resistance, can appear at non-integer Landau level filling fractions. Third, the Hall conductance plateaux remain quantized in integral multiples of e^2/h. However, the quantization integer is not directly associated with the usual Landau level filling fraction. Instead, quantization is equal to the slope of the gap trajectory in the n/n_o–ϕ/ϕ_o Wannier diagram, in accordance with the Diophantine equation (equation (1)).

Minigaps within the fractal energy spectrum become significant only once the magnetic length ($l_B = \sqrt{\hbar/eB}$; $\hbar$, Planck's constant divided by 2π), which characterizes the cyclotron motion, is of the same order as the wavelength of the periodic potential, which characterizes the Bloch waves. For usual crystal lattices, where the interatomic spacing is a few ångströms, the necessary magnetic field is unfeasibly large, in excess of 10,000 T. The main experimental effort therefore has been to lithographically define artificial superlattices[11–17] with unit-cell dimensions of order tens of nanometres, so that the critical magnetic field remains small enough to be achievable in the lab yet still large enough that the QHE is fully resolved without being smeared out by disorder. Fabricating the optimally sized periodic lattice while maintaining coherent registry over the full device and without introducing substantial disorder has proven to be a formidable technical challenge. Patterned GaAs/AlGaAs heterostructures with ~100-nm-period gates provided the first experimental support for the predictions of a Hofstadter spectrum[14–16]. However, limited ability to tune the carrier density or reach the fully developed QHE regime in these samples has made it difficult to map out the complete spectrum. Although similar concepts have been pursued in non-solid-state model systems[20,21], the rich physics of the Hofstadter spectrum remains largely unexplored.

[1]Department of Physics, The City College of New York, New York, New York 10031, USA. [2]Department of Mechanical Engineering, Columbia University, New York, New York 10027, USA. [3]Department of Physics, Columbia University, New York, New York 10027, USA. [4]Department of Physics and Nanoscience Technology Center, University of Central Florida, Orlando, Florida 32816-2385, USA. [5]Department of Physics, Tohoku University, Sendai 980-8578, Japan. [6]National Institute for Materials Science, 1-1 Namiki, Tsukuba 305-0044, Japan. [7]Department of Electrical Engineering, Columbia University, New York, New York 10027, USA.

Heterostructures consisting of atomically thin materials in a multilayer stack provide a new means of realizing a two-dimensional system with a laterally modulated periodic structure. In particular, coupling between graphene and hexagonal boron nitride (hBN), whose crystal lattices are isomorphic, results in a periodic moiré pattern. The moiré wavelength is directly related to the angular rotation between the two lattices[22–24], and can be tuned through the desired length scales without the need for lithographic techniques[8,9]. Moreover, hBN provides an ideal substrate for achieving high-mobility graphene devices, which is crucial for high-resolution quantum Hall measurements[25,26], and field-effect gating in graphene allows the Fermi energy to be continuously varied through the entire moiré Bloch band.

In this study, we used Bernal-stacked bilayer graphene (BLG) Hall bars fabricated on hBN substrates (Fig. 1a, b) using mechanical exfoliation followed by co-lamination (Methods Summary). Figure 1b shows a non-contact atomic force microscopy (AFM) image acquired from an example device. In the magnified region, a triangular moiré pattern is visible with wavelength 15.5 ± 0.9 nm. This is comparable to the maximal moiré wavelength of ~14 nm expected for graphene on hBN[22–24], suggesting that in this device the BLG lattice is oriented relative to the underlying hBN lattice with near-zero angle mismatch.

Figure 1c shows transport data measured from the same device. In addition to the usual resistance peak at the charge neutrality point (CNP), occurring at gate voltage $V_g \approx 2$ V, two additional satellite resistance peaks appear, symmetrically located at $V_{satl} \approx \pm 30$ V relative to the CNP. These satellite features are consistent with a depression in the density of states at the superlattice Brillouin zone band edge, analogous to previous spectroscopic measurements of single-layer graphene coupled to a moiré superlattice[24,27]. Assuming non-overlapping bands, $|V_{satl}|$ gives an estimate of the moiré wavelength of ~14.6 nm (Supplementary Information), in good agreement with the AFM measurements. The nature of these satellite peaks can be further probed in the semiclassical, low-B transport regime. In Fig. 1d, longitudinal resistance, R_{xx}, and transverse Hall resistance, R_{xy}, are plotted versus gate voltage at $B = 1$ T. Near the central CNP, the Hall resistance changes sign as the Fermi energy passes from the electron to the hole band. The same trend also appears near V_{satl}, consistent with the Fermi energy passing through a second band edge. This provides further confirmation that the moiré pattern, acting as a periodic potential superlattice, gives rise to a mini-Brillouin zone band[28]. We observed the satellite peak to be more developed in the hole branch than in the electron branch in all samples, in agreement with previous experimental and theoretical studies of hBN-supported monolayer graphene[24,27,28]. The satellite peaks vanish at temperatures above 100 K (Fig. 1c, inset), indicating that the coupling between the BLG and hBN atomic lattices is of order ~10 meV. Perfect crystallographic alignment between graphene and hBN is expected to open a ~50-meV bandgap[29,30], leading to a low-temperature divergence in the resistance at the CNP. The weak temperature dependence observed in our device suggests the absence of a gap, possibly owing to the lattice mismatch between the BLG and hBN.

In the remainder of this Letter, we focus on magnetotransport measured at high field. Figure 2a shows the evolution of R_{xx} and R_{xy} for magnetic fields up to 31 T. In the left panel (a Landau fan diagram), R_{xx} is plotted against the experimentally tunable gate voltage and magnetic field. In the right panel, the magnitude of the corresponding R_{xy} is plotted against the dimensionless parameters appearing in the Diophantine equation, n/n_o and ϕ/ϕ_o. This Wannier diagram is simply the Landau fan diagram with both axes relabelled by dimensionless units defined by normalizing to the moiré unit-cell area.

In a conventional quantum Hall system, the Landau fan diagram exhibits straight lines, tracking minima in R_{xx} and plateaux in R_{xy}. Plotted against n/n_o and ϕ/ϕ_o, the slope of each line is precisely the Landau level filling fraction, ν, and all lines converge to the origin. White lines in Fig. 2a identify QHE states matching this description, tracking Landau level filling fractions $\nu = 4$, 8 and 12. This is consistent with the usual QHE hierarchy associated with a conventional degenerate BLG spectrum.

At large magnetic fields, several additional QHE states, exhibiting minima in R_{xx} together with plateaux in R_{xy}, develop outside the usual

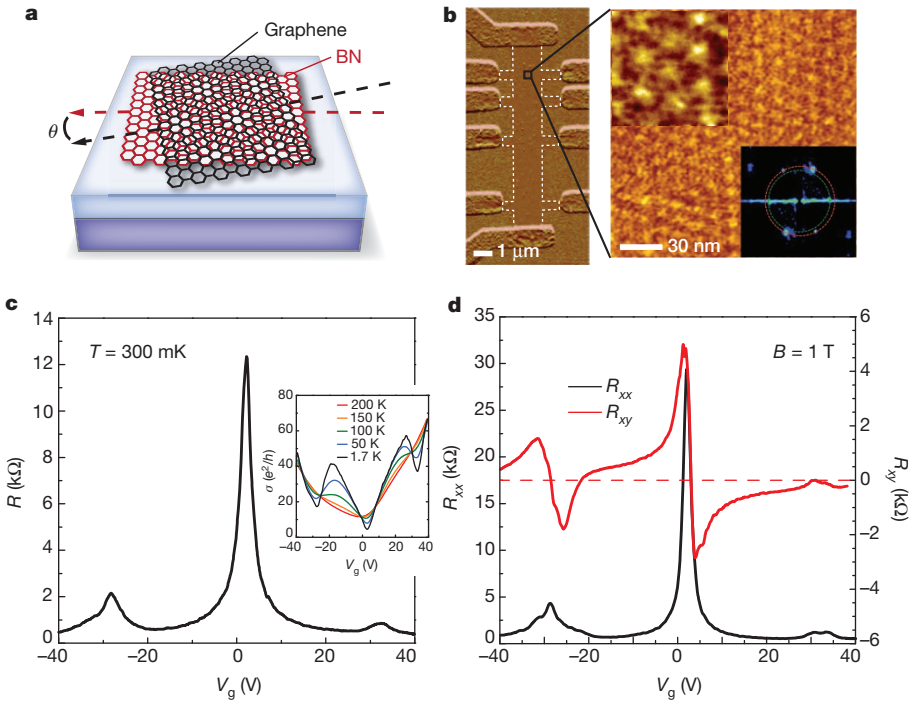

Figure 1 | Moiré superlattice. **a**, Sketch of graphene on hBN showing the emergence of a moiré pattern. The moiré wavelength varies with the mismatch angle, θ. **b**, Left: an AFM image of a multiterminal Hall bar. Right: a high-resolution image of a magnified region. The moiré pattern is evident as a triangular lattice (upper inset shows a further magnified region). A fast Fourier transform of the scan area (lower inset) confirms a triangular lattice symmetry with periodicity 15.5 ± 0.9 nm. **c**, Measured resistance versus gate voltage at zero magnetic field. Inset: the corresponding conductivity versus temperature, indicating that the satellite features disappear at temperatures greater than ~100 K. **d**, Longitudinal resistance (left axis) and Hall resistance (right axis) versus gate voltage at $B = 1$ T. The Hall resistance changes sign and passes through zero at the same gate voltage as the satellite peaks.

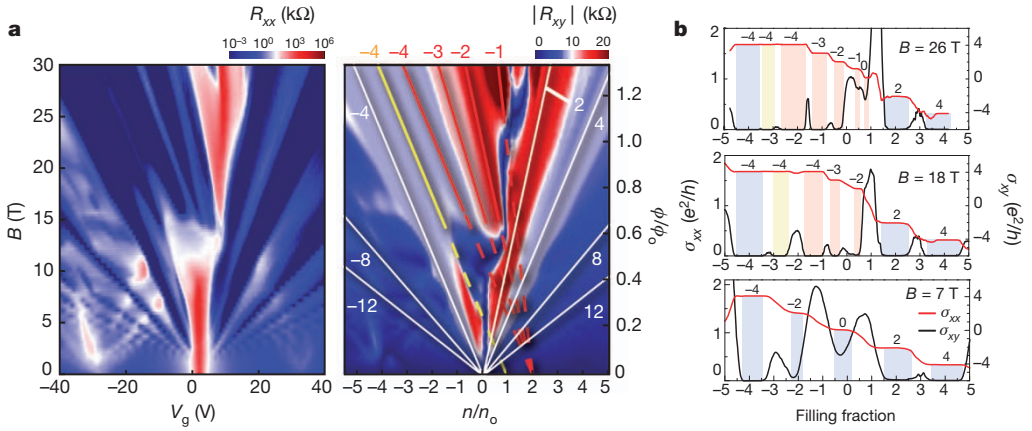

Figure 2 | Emergence of anomalous quantum Hall states. **a**, Landau fan diagram showing longitudinal resistance, R_{xx} (left), and Hall resistance, R_{xy} (right). R_{xx} is plotted versus magnetic field on the vertical axis and versus gate bias on the horizontal axis. In the diagram showing R_{xy}, the axes are scaled by the size of the moiré unit cell to give ϕ/ϕ_o on the vertical axis and n/n_o on the horizontal axis. QHE states corresponding to the conventional BLG spectrum are indicated by white lines. Solid yellow and red lines track the QHE outside this conventional spectrum, with dashed lines indicating the projected n/n_o intercept. The slope of each line is shown on the top axis. **b**, Longitudinal and transverse Hall conductivities corresponding to line cuts at constant magnetic field (constant ϕ/ϕ_o) from the Landau fan diagram in **a**. At $B = 7$ T, the QHE ladder is consistent with previous reports for bilayer graphene. At $B = 18$ and 26 T, additional QHE states emerge, showing Hall conductivity plateaux quantized in integer multiples of e^2/h, but appearing at non-integer Landau level filling fractions. Yellow and red bars indicate correspondence to the similarly coloured anomalous features marked by solid lines in **a**. Blue bars indicate the conventional QHE features. Numbers label the quantization integer for each plateau.

BLG sequence and also follow straight lines in the Landau fan diagram, but converge to non-zero values of n/n_o. Yellow and red lines in Fig. 2a trace examples of these anomalous QHE states appearing within the lowest Landau level. Unlike the conventional QHE states, each of the anomalous QHE states is characterized by both an integer-valued intercept, s (yellow and red lines converge to $n/n_o = 1$ and 2, respectively) and an integer-valued slope, t (labelled along the top axis in the figure). In Fig. 2b, longitudinal and Hall conductivities measured at constant magnetic field (corresponding to horizontal line cuts through the fan diagram in Fig. 2a) are plotted against Landau level filling fraction, ν. At large magnetic fields, the anomalous QHE states are remarkably well developed, exhibiting wide plateaux in σ_{xy} concomitant with $\sigma_{xx} = 0$. Moreover, these states appear in general at non-integer filling fractions. Comparison between Fig. 2a and Fig. 2b further reveals that Hall conductivity plateaux are quantized in integer multiples of e^2/h, where the quantization integer t equals the slope in the Wannier diagram. Similar internal structure is observed within higher-order Landau levels (Fig. 3 and Supplementary Information). The anomalous QHE states observed here are consistent with fully developed spectral gaps resulting from a Hofstadter-type energy spectrum. Moreover, our ability to map fully the density-field space provides a remarkable confirmation of the Diophantine equation: we observe direct evidence that QHE features associated with the Hofstadter spectral gaps are characterized by the two quantum numbers, s and t, corresponding to the n/n_o intercept and the slope, respectively, in the Wannier diagram.

Figure 3 shows similar data to Fig. 2, but measured from a separate device in which the moiré wavelength is only 11.6 nm. Again, QHE states appear outside the conventional Bernal-stacked BLG sequence and follow straight lines whose origin and slope are both integer valued, with the slope exactly matching the Hall quantization, in precise agreement with the Diophantine equation. Similar to the previous device, the $\nu = 0$ insulating state undergoes a drastic change near $\phi/\phi_o = 1/2$, when anomalous QHE states associated with the fractal gaps begin to develop fully.

In Fig. 3b, the lower panel shows σ_{xx} measured at $B = 25$ T, corresponding to a horizontal line cut through Fig. 3a (dashed white line), for a variety of sample temperatures. The magnitudes of the fractal gaps

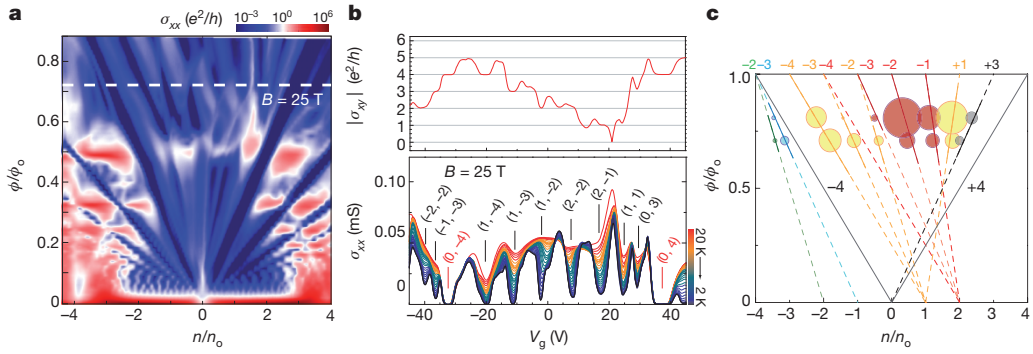

Figure 3 | Fractal gaps. **a**, Landau fan diagrams similar to those in Fig. 2 but measured from a separate device. Here the zero-field satellite peak position indicates a moiré period of 11.6 nm, indicating that the superlattice unit cell was approximately 1.5 times smaller in this device than in the one used in Fig. 2. Significantly more structure is observed here than in Fig. 2. **b**, Bottom: the evolution of σ_{xx} with temperature varying between 2 and 20 K, acquired at constant $B = 25$ T, which corresponds to the line cut shown in **a**. Top: the corresponding σ_{xy} at $T = 2$ K. The bracketed numbers label the (s, t) values of the corresponding fractal gaps according to the Diophantine equation. **c**, Bubble plot of energy gaps determined from the temperature dependence calculated at two magnetic fields ($B = 25$ and 28.5 T). The gaps are plotted as circles with radius scaled relative to the largest gap value measured. Dashed lines trace select fractal gap positions allowed by the Diophantine equation. Solid lines trace regions where the corresponding fractal gaps appear as minima in σ_{xx} together with quantized plateaux in σ_{xy}. The colours indicate gaps with the same quantum number s.

were estimated from the temperature dependence of the σ_{xx} minima in the thermally activated regime (Supplementary Information), at two separate magnetic field values, 25 and 28.5 T. Figure 3c summarizes our findings. Each fractal gap is marked by a circle centred at the corresponding $(n/n_o, \phi/\phi_o)$ coordinates, and with radius scaled relative to the largest gap value (Supplementary Information). As the magnetic field increases, the spectral energies develop in a complicated way: some gaps grow with field (for example those with $(s, t) = (1, 1)$ and $(2, -2)$), whereas others shrink (for example $(1, -4)$). For a fixed magnetic field, it seems generally true that for constant s values, fractal gap states exhibit increasing gap size as t increases. For example, at $B = 25$ T, $\Delta_{(1,-4)} \approx 48$ K whereas $\Delta_{(1,-3)} \approx 30$ K. This contradicts the prediction that fractal gaps corresponding to lower quantum numbers have larger gap values[1]. We note that such a trend was subsequently found to be specific to square lattice symmetries[2,5]. Furthermore, a non-trivial case also arises when two fractal gap states overlap[2], such as occurs between the $(1, -2)$ and $(2, -3)$ states in our data as $\phi/\phi_o \rightarrow 1$. Further theoretical analysis specific to moiré-patterned BLG is necessary to understand fully the trends highlighted here.

Figure 4a shows a normalized Landau fan diagram of R_{xy} values corresponding to the R_{xx} data in Fig. 3a. Dashed horizontal lines in the figure label special values of the normalized magnetic flux, $\phi/\phi_o = 1/m$, where m is integer valued. Referred to as the 'pure cases'[1], these lines of high symmetry provide the framework for the recursive structure of the butterfly spectrum, marking the boundaries of the repeating sub-cells that appear within the main cell[5]. In Fig. 4a, at the pure cases in the fan diagram, R_{xy} seems to tend to zero and change sign. This is also seen from the single line trace in Fig. 4b. In the quantum Hall regime, the longitudinal conductivity has a local peak as the magnetic field passes through the pure cases, with the corresponding Hall conductivity exhibiting a sharp transition. For large magnetic fields, both of these features span the full Landau level along lines of constant ϕ/ϕ_o, as seen in Figs 3a and 4a, respectively. Near the field corresponding to $\phi/\phi_o = 1/2$, labelled in Fig. 4c as $B_{1/2}$, plateaux appear in R_{xy} together with minima in R_{xx}, resembling a mini QHE series centred on $B_{1/2}$. If we redefine the local effective magnetic field as $B' = B - B_{1/2}$, then, according to the usual QHE formalism, we expect to find that $\nu' = (1/B')n'h/e$, where ν' is an effective filling fraction given by the Hall quantization, B' is the value of the effective magnetic field at the R_{xx} minima and n' is an effective carrier density. The inset in Fig. 4c shows a plot of ν' versus $1/B'$ and the data indeed follows a linear trend. In spite of the large magnetic field ($B_{1/2} \approx 17.3$ T), this indicates that locally the electrons behave as if the magnetic field is reduced to zero. We regard this as compelling evidence of the long-predicted recursive nature of the Hofstadter spectrum, where repeated mini fan diagrams emerge within the main one. We note that the linear trend shown inset in Fig. 4c does not pass through the origin, but is vertically offset by 4.1 ± 0.1. The origin of this offset is unclear but may be related to disorder effects because in this regime the spectrum is not fully gapped[6].

Finally, we note that precise modelling of the fractal spectrum (Supplementary Information) requires a quantitative understanding of the atomic-scale couplings between BLG and hBN and between the BLG layers, which are not well known. Additionally the odd-integer quantum numbers observed in our experiment, which may not be accounted for in a purely single-particle picture, invite further investigation of correlated electron behaviour within the Hofstadter spectrum.

In conclusion, we report experimental confirmation that the generalized behaviour of electrons subjected simultaneously to both a magnetic field and a spatially varying periodic electrostatic field is described by a Diophantine equation involving two topological quantum numbers. The ability to tune the competing length scales governing these Landau–Bloch–Dirac states in graphene coupled to a substrate-induced

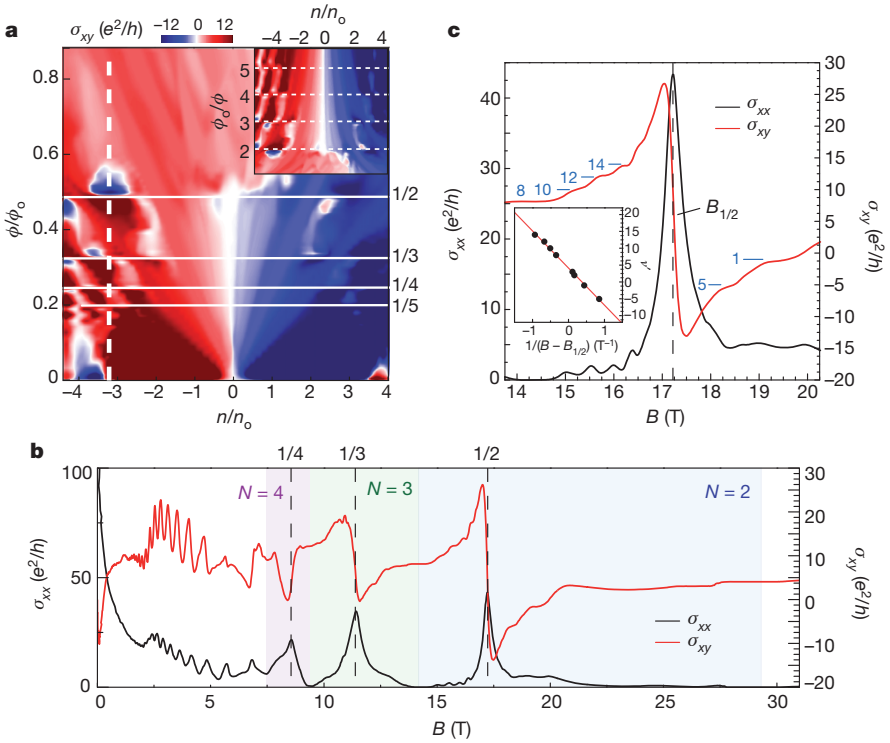

Figure 4 | Recursive structure. **a**, R_{xy} Wannier diagram for the device used in Fig. 3. White solid lines label ϕ/ϕ_o values corresponding to the pure cases, $\phi/\phi_o = 1/m$. Inset: data replotted against ϕ_o/ϕ, illustrating that the main experimental features exhibit a $1/B$ periodicity. **b**, Longitudinal conductivity, σ_{xx} (left axis), and Hall conductivity, σ_{xy} (right axis), versus magnetic field, measured at a constant gate voltage ($V_g = -39$ V, corresponding to the white dashed line in **a**). Blue, green and purple bands mark the boundaries of the conventional $N = 2$, 3 and 4 Landau levels, respectively. Dashed lines mark the values of B corresponding to the pure fractions labelled in **a**. The values of ϕ/ϕ_o are shown on the top axis. **c**, Details of both σ_{xx} and σ_{xy} in the vicinity of $\phi/\phi_o = 1/2$ (**b**). Plateaux in σ_{xy} concomitant with minima in σ_{xx} resemble a mini QHE trace centred on $\phi/\phi_o = 1/2$, consistent with the prediction of recursion in the butterfly spectrum[1]. Inset: the positions of the mini QHE plateaux plotted versus effective magnetic field follow a linear trend (see text).

moiré superlattice makes it possible to study experimentally the complexity of the Hofstadter energy spectrum and, in particular, to investigate the role of electron interactions within it.

METHODS SUMMARY

Using a co-lamination mechanical transfer technique similar to that described previously[25,26], graphene–hBN stacks were fabricated on doped Si substrates with a ~300-nm oxide layer. Each stack was then etched into a Hall bar with evaporated Cr/Pd/Au leads using standard electron-beam lithography processes. The bottom boron nitride layer was chosen to be between 10 and 20 nm thick. More than 20 devices were made in this way, with six devices showing similar behaviour to that reported here. We focus only on two high-quality devices in the text, listing other examples in Supplementary Information. The device shown in Fig. 1b represents a typical Hall bar geometry with a channel width of 1 μm and spacing between voltage probes varying from 1 to ~4 μm. Identical transport features were measured across all voltage probes, indicating that the moiré pattern exhibits good uniformity over the entire length of the device. Mobility in our devices ranged from approximately 10,000 to 100,000 $cm^2 V^{-1} s^{-1}$, as estimated by fitting a Boltzmann model to the linear response. Four-terminal transport measurements were performed using a lock-in amplifier at 17 Hz with a 10–100-nA source current, using the doped silicon substrate to gate the channel. Samples were measured in a 31-T resistive magnet and a ^{3}He cryostat (sample in vapour). Longitudinal and Hall conductivities were calculated from the measured resistances according to $\sigma_{xx} = \rho_{xx} \Big/ \left(\rho_{xx}^2 + R_{xy}^2\right)$ and $\sigma_{xy} = R_{xy} \Big/ \left(\rho_{xx}^2 + R_{xy}^2\right)$, respectively.

AFM images of the device were acquired at room temperature, using an Omicron low-temperature AFM system. Imaging was performed using a bias voltage of $V_{bias} = 0.2$ V and frequency shift of $\delta f = 20$ Hz. Images were filtered to remove noise.

Received 13 December 2012; accepted 3 April 2013.
Published online 15 May 2013.

1. Hofstadter, D. Energy levels and wave functions of Bloch electrons in rational and irrational magnetic fields. *Phys. Rev. B* **14,** 2239–2249 (1976).
2. Wannier, G. H. A result not dependent on rationality for Bloch electrons in a magnetic field. *Phys. Status Solidi B* **88,** 757–765 (1978).
3. Středa, P. Quantised Hall effect in a two-dimensional periodic potential. *J. Phys. C* **15,** L1299–L1303 (1982).
4. Thouless, D., Kohmoto, M., Nightingale, M. & den Nijs, M. Quantized Hall conductance in a two-dimensional periodic potential. *Phys. Rev. Lett.* **49,** 405–408 (1982).
5. MacDonald, A. Landau-level subband structure of electrons on a square lattice. *Phys. Rev. B* **28,** 6713–6717 (1983).
6. Koshino, M. & Ando, T. Hall plateau diagram for the Hofstadter butterfly energy spectrum. *Phys. Rev. B* **73,** 155304 (2006).
7. Nemec, N. & Cuniberti, G. Hofstadter butterflies of bilayer graphene. *Phys. Rev. B* **75,** 201404(R) (2007).
8. Bistritzer, R. & MacDonald, A. Moiré butterflies in twisted bilayer graphene. *Phys. Rev. B* **84,** 035440 (2011).
9. Moon, P. & Koshino, M. Energy spectrum and quantum Hall effect in twisted bilayer graphene. *Phys. Rev. B* **85,** 195458 (2012).
10. Beugeling, W., Goldman, N. & Morais Smith, C. Topological phases in a two-dimensional lattice: magnetic field versus spin-orbit coupling. *Phys. Rev. B* **86,** 075118 (2012).
11. Gerhardts, R., Weiss, D. & Wulf, U. Magnetoresistance oscillations in a grid potential: indication of a Hofstadter-type energy spectrum. *Phys. Rev. B* **43,** 5192–5195 (1991).
12. Nakamura, Y., Inoshita, T. & Sakaki, H. Novel magneto-resistance oscillations in laterally modulated two-dimensional electrons with 20nm periodicity formed on vicinal GaAs (111)B substrates. *Physica E* **2,** 944–948 (1998).
13. Albrecht, C. *et al.* Fermiology of two-dimensional lateral superlattices. *Phys. Rev. Lett.* **83,** 2234–2237 (1999).
14. Schlösser, T., Ensslin, K., Kotthaus, J. P. & Holland, M. Landau subbands generated by a lateral electrostatic superlattice: chasing the Hofstadter butterfly. *Semicond. Sci. Technol.* **11,** 1582–1585 (1996).
15. Albrecht, C. *et al.* Evidence of Hofstadter's fractal energy spectrum in the quantized Hall conductance. *Phys. Rev. Lett.* **86,** 147–150 (2001).
16. Geisler, M. C. *et al.* Detection of Landau band coupling induced rearrangement of the Hofstadter butterfly. *Physica E* **25,** 227–232 (2004).
17. Melinte, S. *et al.* Laterally modulated 2D electron system in the extreme quantum limit. *Phys. Rev. Lett.* **92,** 036802 (2004).
18. Harper, P. G. Single band motion of conduction electrons in a uniform magnetic field. *Proc. Phys. Soc. A* **68,** 874–878 (1955).
19. von Klitzing, K., Dorda, G. & Pepper, M. New method for high-accuracy determination of the fine-structure constant based on quantized Hall resistance. *Phys. Rev. Lett.* **45,** 494–497 (1980).
20. Kuhl, U. & Stöckmann, H. J. Microwave realization of the Hofstadter butterfly. *Phys. Rev. Lett.* **80,** 3232–3235 (1998).
21. Jaksch, D. & Zoller, P. Creation of effective magnetic fields in optical lattices: the Hofstadter butterfly for cold neutral atoms. *N. J. Phys.* **5,** 56 (2003).
22. Xue, J. *et al.* Scanning tunnelling microscopy and spectroscopy of ultra-flat graphene on hexagonal boron nitride. *Nature Mater.* **10,** 282–285 (2011).
23. Decker, R. *et al.* Local electronic properties of graphene on a BN substrate via scanning tunneling microscopy. *Nano Lett.* **11,** 2291–2295 (2011).
24. Yankowitz, M. *et al.* Emergence of superlattice Dirac points in graphene on hexagonal boron nitride. *Nature Phys.* **8,** 382–386 (2012).
25. Dean, C. R. *et al.* Boron nitride substrates for high-quality graphene electronics. *Nature Nanotechnol.* **5,** 722–726 (2010).
26. Dean, C. R. *et al.* Multicomponent fractional quantum Hall effect in graphene. *Nature Phys.* **7,** 693–696 (2011).
27. Li, G. *et al.* Observation of Van Hove singularities in twisted graphene layers. *Nature Phys.* **6,** 109–113 (2010).
28. Wallbank, J. R., Patel, A. A., Mucha-Kruczynski, M., Geim, A. K. & Fal'ko, V. I. Generic miniband structure of graphene on a hexagonal substrate. Preprint at http://arxiv.org/abs/1211.4711 (2012).
29. Giovannetti, G., Khomyakov, P., Brocks, G., Kelly, P. & Van Den Brink, J. Substrate-induced band gap in graphene on hexagonal boron nitride: ab initio density functional calculations. *Phys. Rev. B* **76,** 073103 (2007).
30. Ramasubramaniam, A., Naveh, D. & Towe, E. Tunable band gaps in bilayer graphene-BN heterostructures. *Nano Lett.* **11,** 1070–1075 (2011).

Supplementary Information is available in the online version of the paper.

Acknowledgements We thank A. MacDonald for discussions. A portion of this work was performed at the National High Magnetic Field Laboratory, which is supported by US National Science Foundation cooperative agreement no. DMR-0654118, the State of Florida and the US Department of Energy. This work is supported by AFOSR MURI. J.K. and M.I. were supported by the US National Science Foundation under grant no. 0955625. K.L.S. was supported by DARPA under Office of Naval Research contract N00014-1210814. P.K. and F.G. acknowledge sole support from the US Department of Energy (DE-FG02-05ER46215).

Author Contributions C.R.D., P. Maher, L.W., C.F., F.G. and Y.G. performed device fabrication and transport measurements. J.K. and M.I. performed AFM measurements. P. Moon and M.K. provided theoretical support. K.W. and T.T. synthesized the hBN samples. K.L.S., J.H. and P.K. advised on experiments. C.R.D., P. Maher, P. Moon, M.K., J.H. and P.K. wrote the manuscript in consultation with all other authors.

Author Information Reprints and permissions information is available at www.nature.com/reprints. The authors declare no competing financial interests. Readers are welcome to comment on the online version of the paper. Correspondence and requests for materials should be addressed to P.K. (pk2015@columbia.edu).